JOURNAL OF AIRCRAFT
Vol. 45, No. 3, May–June 2008

Wing-Rock Limit Cycle Oscillation Prediction Based on Computational Fluid Dynamics

K. J. Badcock* and M. A. Woodgate†
University of Liverpool, Liverpool, England L69 3BX, United Kingdom
M. R. Allan‡
University of Glasgow, Glasgow, Scotland G12 8QQ, United Kingdom
and
P. S. Beran§
U.S. Air Force Research Laboratory, Wright-Patterson Air Force Base, Ohio 45433-7531

DOI: 10.2514/1.32812

The investigation of flight dynamics instability, when based on computational fluid dynamics level aerodynamics, is traditionally done in the time domain. It is, however, possible to look to the behavior of the eigenspectrum of the Jacobian of the semidiscrete system to obtain information at a reduced computational cost. The central computational task in this approach is to solve a sparse linear system, with a key issue being the calculation of an effective parallel preconditioner. With a knowledge of the bifurcation angle and the critical eigenvalue/eigenvector, it is possible to develop a reduced-order model which can predict the limit cycle amplitude postbifurcation. In this paper the shifted inverse power method, built on a preconditioned sparse matrix solver, is used to predict the wing-rock onset angle of an 80-deg delta wing. The postbifurcation limit cycle oscillations are then calculated using a reduced model which uses knowledge of the critical mode of the system. This problem is considered here as a prototype flight dynamics instability.

Nomenclature

A	=	Jacobian matrix of $\mathbf{R}$ with respect to $\mathbf{w}$
B, C	=	second and third Jacobian operators
c_r	=	root chord
G	=	Taylor coefficients of the residual restricted into the critical eigenspace
H	=	Taylor coefficients of the residual restricted into the noncritical eigenspace
h	=	(scalar) increment for finite differences
I_{xx}	=	rolling moment of inertia
k_{ij}	=	coefficients in center manifold expansion of y
M	=	inverse of A approximated by the polynomial preconditioner
$\mathbf{p} = \mathbf{p}_1 + i\mathbf{p}_2$	=	right eigenvector of A
$\mathbf{q} = \mathbf{q}_1 + i\mathbf{q}_2$	=	left eigenvector of A
$\mathbf{R}$	=	residual vector
s	=	polynomial used for preconditioner
$\mathbf{w}$	=	vector of unknowns
$\mathbf{x}$	=	grid locations
y	=	the part of $\mathbf{w}$ in the noncritical eigenspace
z	=	the part of $\mathbf{w}$ in the critical eigenspace
λ_i	=	sequence of eigenvalues in inverse power method
μ	=	$\mu = \rho_\infty c_r^5 / I_{xx}$
ρ_∞	=	freestream density
ϕ	=	roll angle
ω	=	frequency of critical eigenvalue or shift for inverse power method

Subscripts

a	=	fluid model
f	=	structural model
i, j	=	flux interface i, j
l	=	left interpolated value at an interface
r	=	right interpolated value at an interface
$\mathbf{w}$	=	indicating differentiation with respect to $\mathbf{w}$
0	=	equilibrium solution or initial grid location

Superscripts

$\bar{\mathbf{p}}$, $\bar{\mathbf{q}}$, $\bar{z}$	=	complex conjugate
$\bar{\mathbf{w}}$, $\bar{\alpha}$	=	difference from equilibrium solution

Introduction

ROLLING motion about the longitudinal axis of a delta wing has been computed using computational fluid dynamics (CFD) by several researchers [1–4]. Recently, a comprehensive numerical study of the wing rock was conducted by Saad [5] using a 3 deg-of-freedom flight mechanics model for a generic fighter aircraft configuration (forebody, 65-deg leading-edge sweep, and vertical fin). Roll, sideslip, and vertical degrees of freedom were included. Including the sideslip degree of freedom was found to delay the onset of the wing rock and reduce the wing-rock amplitude. These problems provide a useful test case for computing flight mechanics instability because they feature the simplicity of constrained motions and the complexity of nonlinear aerodynamics.

The computational cost of time domain CFD based predictions can be high. A way of reducing the cost of computing parametric searches for aeroelastic stability was proposed by Morton and Beran [6]. Their method uses dynamical systems theory to characterize the nature of the aeroelastic instability, with this additional information concentrating the use of the CFD. In this way the problem of locating

Received 14 June 2007; revision received 8 August 2007; accepted for publication 12 August 2007.

*Professor, Computational Fluid Dynamics Laboratory, Flight Sciences and Technology, Department of Engineering; K.J.Badcock@liverpool.ac.uk. Member AIAA (Corresponding Author).

†Research Assistant, Computational Fluid Dynamics Laboratory, Flight Sciences and Technology, Department of Engineering.

‡Research Assistant, Computational Fluid Dynamics Laboratory, Department of Aerospace Engineering.

§Principal Research Aerospace Engineer, Multidisciplinary Technologies Center.

a one-parameter Hopf bifurcation was reduced from multiple time marching calculations to a single steady-state calculation of a modified (or augmented) system. This augmented system, solved via Newton's method, calculates the value of the bifurcation parameter for which an eigenvalue of the system Jacobian matrix crosses the imaginary axis.

This approach has also been applied to compute wing-rock onset angles [7]. The formulation used a sparse matrix solver to efficiently solve the linear system arising at each Newton step for the augmented system. A matrix free product was used to evaluate the Jacobian-vector product for the augmented residual, resulting in convergence to the correct wing-rock onset angle for a spatial discretization of second-order accuracy. However, the Newton iterations were driven to convergence by the Jacobian matrix of the first-order scheme, leading to a loss of quadratic convergence. Note that the Jacobian matrix we refer to is of the coupled CFD-rolling motion system of equations, and so involves the derivatives of the CFD spatial discretization (here based on Osher's approximate Riemann solver).

The classical shifted inverse power method (IPM) can be applied to the Jacobian matrix at any angle of attack to compute the critical pair of eigenvalues. This is useful to derive a starting solution for the augmented solver, and is a fast method for finding the onset angle in its own right. However, because only the Jacobian of the first-order spatial scheme was available in the previous work it was not possible to exploit the full capability of the IPM.

Recently the analytical Jacobian for the second-order spatial discretization was derived and coded [8]. This opened up the possibility of applying the IPM to calculate stability. This is exploited in the current paper for predicting the wing-rock onset angle.

The computational work involved with the IPM is largely associated with the linear solver. A key consideration for tackling full aircraft problems, with their significant requirements for grid points and CPU time, is the implementation of the IPM on a distributed memory parallel computer. The generation of residuals and Jacobians can be done effectively in parallel without much difficulty. The same is not true for the solution of sparse linear systems. A key point considered in this paper is the development of an acceptable distributed preconditioner for Krylov-type methods.

The postbifurcation response of wing rock is a limit cycle oscillation. Knowledge of the onset angle is important, but the growth in the magnitude of the oscillation after the onset angle has been passed is also key information. The limit cycle response of an aeroelastic system was predicted [8] using a projection onto the critical mode calculated from the IPM. A 2-degree-of-freedom equation was obtained that very successfully predicted the full-order response of a flexible wing-store configuration driven by a shock wave motion. This method is adapted in the current paper for predicting wing-rock limit cycle amplitudes.

The paper continues with a summary of the formulation of the model and IPM. Then the linear solver is presented for parallel calculations. The reduced-order model is then described. Finally, results are presented to illustrate the performance of these methods.

Formulation

Model

The coupled rolling motion/Euler equations can be written to emphasize the dependencies as

$$\frac{\mathrm{d}}{\mathrm{d}t}\begin{bmatrix}\mathbf{w}_a\\ \phi_t\\ \phi\end{bmatrix}=\begin{bmatrix}\mathbf{R}_a(\mathbf{w}_a,\phi,\phi_t,\alpha)\\ \mu C_{l_c}(\mathbf{w}_a)+D\phi_t\\ \phi_t\end{bmatrix}$$

Here the vector $\mathbf{R}_a$ denotes the discretization of the spatial terms in the Euler equations, the details of which follow the formulation described in [9], which can be summarized as discretization using Osher's method with monotone upwind scheme for conservation laws (MUSCL) interpolation on moving multiblock meshes. Writing this system in the form

$$\frac{\partial \mathbf{w}}{\partial t}=\mathbf{R}$$

the stability of an equilibrium $\mathbf{w}=\mathbf{w}_0$ which satisfies $\mathbf{R}(\mathbf{w}_0)=\mathbf{0}$ is determined by the eigensystem of the Jacobian matrix $A=\partial\mathbf{R}/\partial\mathbf{w}$. The matrix can be written out in block format as

$$A=\begin{bmatrix}\frac{\partial \mathbf{R}_a}{\partial \mathbf{w}_a} & \frac{\partial \mathbf{R}_a}{\partial \phi_t} & \frac{\partial \mathbf{R}_a}{\partial \phi}\\ \mu\frac{\partial C_{l_c}}{\partial \mathbf{w}_a} & D & 0\\ 0 & 1 & 0\end{bmatrix}=\begin{bmatrix}A_{aa} & A_{af}\\ A_{fa} & A_{ff}\end{bmatrix} \tag{1}$$

The term A_{aa} is a large sparse matrix which represents the Jacobian of the discretization of the fluid equations with respect to the fluid variables. The details of the calculation of A_{aa} are given in [8]. In summary, the calculation is made in two parts. First, the derivatives of the fluxes computed by Osher's flux function with respect to the left and right interface values are calculated. Next, the derivatives of the interface values on the adjacent cell-centered values are computed. These are combined through the chain rule to assemble the cell residual Jacobians with respect to adjacent cell values. All these calculations have been coded analytically.

For A_{fa} the rolling moment depends linearly on the surface pressures, which in turn depend linearly on the pressure values in the two internal cells adjacent to the boundary. The term A_{af} is derived from noting that, if initially $\phi=0$ and the grid is at $\mathbf{x}_0$, and the body axis points along the x axis, then the instantaneous grid locations are

$$\mathbf{x}=\begin{bmatrix}1 & 0 & 0\\ 0 & \cos\phi & -\sin\phi\\ 0 & \sin\phi & \cos\phi\end{bmatrix} \tag{2}$$

The grid speeds are then

$$\mathbf{x}_t=\phi_t\begin{bmatrix}0 & 0 & 0\\ 0 & -\sin\phi & -\cos\phi\\ 0 & \cos\phi & -\sin\phi\end{bmatrix} \tag{3}$$

The terms in A_{af} are then calculated through finite differences by incrementing ϕ or ϕ_t, evaluating $\mathbf{x}$ if ϕ has been incremented or $\mathbf{x}_t$ if ϕ_t has been incremented, updating the body boundary conditions and then recalculating the aerodynamic residual for the finite difference calculation. Finally A_{ff} can be calculated analytically.

Stability Calculation

We consider the stability problem with the angle of attack α as the parameter. We are interested in finding the onset angle for the wing rock and assume that stability is lost through a Hopf bifurcation. In this case the Jacobian matrix A has a pair of purely imaginary eigenvalues at the critical angle.

The power method [10] is an algorithm for calculating the dominant eigenvalue/eigenvector pair of a diagonalizable matrix A. Its extension to the shifted inverse power method (IPM) is practical for finding any eigenvalue provided that a good initial approximation is known. Assume that the $n\times n$ matrix A has distinct eigenvalues $\lambda_1,\lambda_2,\ldots,\lambda_n$ and consider the eigenvalue λ_j. Then a constant ω can be chosen so that $1/(\lambda_j-\omega)$ is the dominant eigenvalue of the matrix $(A-\omega I)^{-1}$.

The IPM can be used to calculate the location of the critical eigenvalue in the complex plane at a fixed angle α. By computing the location for multiple values of α, the angle at which the eigenvalue crosses the imaginary axis can be computed. Variations on this approach are possible and are formulated in detail in [7].

Linear Solver

A key part of the computational work in the IPM is the solution of a large sparse linear system. Eisenstat et al. [11] developed a generalized conjugate gradient method that depends only on A, and is called the generalized conjugate residual (GCR) algorithm. Saad and Schultz developed the generalized minimal residual (GMRES) algorithm which is mathematically equivalent to GCR but is less

prone to break down for certain problems and requires less storage and arithmetic operations. However, GCR remains the easier algorithm to implement, especially in parallel.

It is crucial for an iterative linear solver to have an effective preconditioner. The basic method used in the current work is the block incomplete lower–upper (BILU) factorization. An approximate factorization of the coefficient matrix into lower and upper factors is calculated, with the sparsity pattern of the factorization restricted according to an algorithm that allows the calculation of progressively better approximations to the exact inverse, at the cost of including more terms (levels) in the factors. The case where the sparsity pattern of the factors is the same as the original Jacobian matrix is referred to as level 0, or BILU(0). The subsequent levels of fill-in are given integer values, level k or BILU(k).

There are two variations of the linear solver used in the current work. Real and complex variable versions of the linear solver have been coded. A complex variable formulation has three advantages over splitting the variable into real and imaginary parts. First, the bandwidth of the matrix is not expanded. Second, the preconditioner is faster to calculate and requires less storage. Third, the preconditioner was found to be more robust with respect to dropping off-diagonal terms.

A key development for making the IPM a practical proposition for full-scale problems is the development of a parallel implementation of the method. Calculating the steady state and forming the Jacobian matrix are standard operations. The data decomposition is done by storing whole blocks of the multiblock grid on a single processor. This means that the partitioning of the grid can be considered as a problem of assigning blocks to processors. Each processor stores a certain number of blocks in the grid and their associated fluid variables. The structural variables are treated in a different way. Each processor stores all the structural information. This is not expensive for the current problem. The residual and Jacobian are decomposed as shown in Fig. 1.

Now, the crucial issue is the parallel implementation of the linear solver. The calculation of the lower–upper (LU) factors and the forward and backward substitutions on these factors are both sequential operations. It is possible to ignore terms in the Jacobian matrix A which couple the system between processors. However, this can have a very bad influence on the convergence of the Krylov iterations for the systems being considered in the IPM. The decoupling of blocks through dropping terms localizes the approximation to the solution of the linear system.

To improve the coupling between processors at the preconditioning stage a polynomial preconditioner was considered. In polynomial preconditioning the matrix M is defined by

$$M^{-1} = s(A)$$

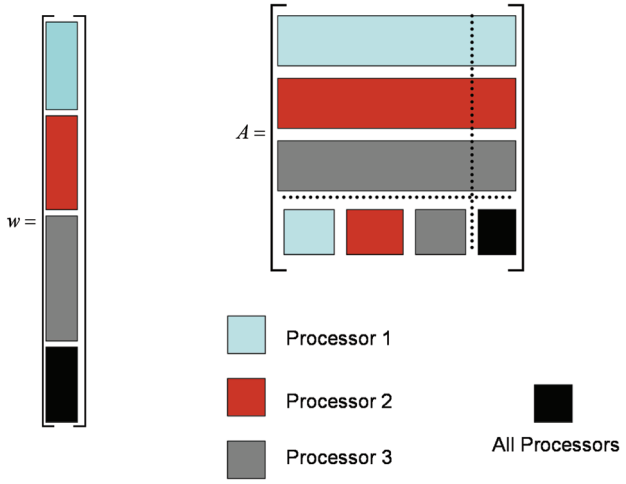

Fig. 1 Schematic of the data decomposition, for a 3-processor calculation, of the Jacobian and right-hand side vector.

where s is a low degree polynomial. The polynomial s is derived from the Neumann series expansion

$$s(A) = I + N + N^2 + N^3 + \cdots + N^s$$

where $N = I - A$. Then

$$M^{-1}A = (I - N^{s+1})$$

An efficient parallel implementation of this preconditioner is possible because it consists of matrix–vector products.

The option finally selected for the preconditioner uses a combination of the localized BILU preconditioner with the first-order polynomial preconditioner. The idea is that the polynomial preconditioner brings in some of the global information through matrix–vector products that is lost by the localization of the BILU factorization, with both stages being effective in parallel.

Model Reduction

The bifurcation angle is computed using the IPM. This calculation also gives the imaginary part of the critical eigenvalue and the corresponding eigenvector. We can also compute the eigenvector of the transpose of the Jacobian matrix using the IPM. This information can be used to develop a reduced model for predicting the limit cycle response at angles higher than the bifurcation angle.

The basic approach is based on the observation that the system responds in the critical mode close to the bifurcation angle. The full-order system unknowns are projected onto the critical mode to give the 2 (i.e., complex) degrees of freedom that are critical to the system dynamics. The full-order model is also projected onto the critical mode. The residual is expanded in a Taylor series, retaining quadratic and cubic terms. The second and third Jacobians do not have to be explicitly formed, because it is only their action on vectors that is required. Hence, matrix free products and extended order arithmetic are used to obtain accurate approximations. Finally, the influence of the noncritical space on the critical mode is included through a center manifold approximation.

The result is two scalar equations which predict the response of the critical mode, and the response of the full-order system can be reconstructed from the critical coordinates. These equations are obtained at the cost of solving three linear systems and a few extended order arithmetic matrix–vector products.

Finally, and importantly, the scalar equations are parameterized through a Taylor expansion in the angle of attack, with the higher order derivatives obtained through finite difference approximations.

The algorithmic details are given by the following steps:

1) Calculate α_0, $\mathbf{p}$, $\mathbf{q}$, and ω from the IPM solver. Here $\mathbf{q}$ is the critical right eigenvector of the Jacobian matrix, $\mathbf{p}$ is the critical right eigenvector of the transpose of the Jacobian matrix, α_0 is the wing-rock onset angle, and $\pm i\omega$ is the critical eigenvalue.

2) Calculate $B(\mathbf{q}, \bar{\mathbf{q}})$ and $B(\mathbf{q}, \mathbf{q})$. Here B is the second Jacobian operator

$$B(\mathbf{w}_1, \mathbf{w}_2) = \frac{1}{2}\frac{\partial^2 R}{\partial w^2}\mathbf{w}_1\mathbf{w}_2$$

3) Solve

$$\begin{cases} (2i\omega I - A)h_{20} = B(\mathbf{q}, \mathbf{q}) \\ Ah_{11} = B(\mathbf{q}, \bar{\mathbf{q}}) \end{cases} \tag{4}$$

4) Form $C(\mathbf{q}, \mathbf{q}, \bar{\mathbf{q}})$. Here

$$C(\mathbf{w}_1, \mathbf{w}_2, \mathbf{w}_3) = \frac{1}{6}\frac{\partial^3 R}{\partial w^3}\mathbf{w}_1\mathbf{w}_2\mathbf{w}_3$$

is the third Jacobian operator.

5) Form g_{20}, g_{11}, and g_{21}, where

$$g_{20} = \langle \mathbf{p}, B(\mathbf{q}, \mathbf{q}) \rangle \qquad g_{11} = \langle \mathbf{p}, B(\mathbf{q}, \bar{\mathbf{q}}) \rangle$$

and

$$g_{21} = \langle \mathbf{p}, C(\mathbf{q}, \mathbf{q}, \bar{\mathbf{q}}) \rangle - 2\langle \mathbf{p}, B(\mathbf{q}, A^{-1}B(\mathbf{q}, \bar{\mathbf{q}})) \rangle + \langle \mathbf{p}, B(\bar{\mathbf{q}}, (2i\omega I - A)^{-1}B(\mathbf{q}, \mathbf{q})) \rangle + \frac{1}{i\omega}\langle \mathbf{p}, B(\mathbf{q}, \mathbf{q}) \rangle \langle \mathbf{p}, B(\mathbf{q}, \bar{\mathbf{q}}) \rangle - \frac{2}{i\omega}|\langle \mathbf{p}, B(\mathbf{q}, \bar{\mathbf{q}}) \rangle|^2 - \frac{1}{3i\omega}|\langle \mathbf{p}, B(\bar{\mathbf{q}}, \bar{\mathbf{q}}) \rangle|^2$$

6) Calculate the terms from the parameter expansion

$$\alpha_{00} = \left\langle \mathbf{q}, \frac{\partial \mathbf{R}}{\partial \alpha} \right\rangle \qquad \alpha_{01} = \langle \mathbf{q}, A_\alpha \mathbf{p} \rangle \qquad \alpha_{10} = \langle \mathbf{q}, A_\alpha \bar{\mathbf{p}} \rangle$$

Note that the terms arising from

$$\alpha_2 = \langle \mathbf{q}, A_\alpha \mathbf{y} \rangle$$

lead to quadratic terms in z and $\bar{z}$ after exploiting the center manifold expression. These terms were found to be small and so were approximated as zero in the final calculations.

7) Time march

$$\dot{\bar{z}} = i\omega z + \tfrac{1}{2}g_{20}z^2 + g_{11}z\bar{z} + \tfrac{1}{2}g_{02}\bar{z}^2 + \tfrac{1}{2}g_{21}z^2\bar{z} + \hat{\alpha}(\alpha_{00} + \alpha_{01}z + \alpha_{10}\bar{z})$$

For the implementation a number of issues were tackled. First, the parameter terms, including the term A_α, were calculated. This was done using finite differences, requiring only two residual evaluations [8]. The evaluation of these finite differences suffers from the truncation error for values of the step size h which are too large, and from the rounding error for values which are too small. To overcome the second limit, quad-double arithmetic was used for the residual evaluation. A high precision version of algebraic and transcendental functions is also required, in this case because of the contributions of such functions in Osher's flux function. The Quad-Double (QD) library[¶] was used to obtain this functionality. This library allows extension of existing code to double–double precision and quad–double precision without major recoding, by using operator overloading.

To test the accuracy of the reduced model terms, the convergence of the third Jacobian term, for the second-order spatial discretization, with h, is considered. The third Jacobian term is more sensitive to the rounding error than the second Jacobian or parameter terms. The convergence is shown in Table 1 and there is a good range of values for h where satisfactory convergence is obtained.

Test Case and Time Marching Results

Test Case Description

There is a considerable amount of published experimental data for 80-deg sweep delta wings, and so this sweep angle was selected for the current study. The geometry of the wing was identical to that used by Arena and Nelson [12]. The sharp leading-edge wing has a flat upper and lower surface with a 45-deg windward bevel and a root chord of 0.4222 m. The moment of inertia for this wing was given as $I_{xx} = 0.00125\ \text{kg} \cdot \text{m}^2$. The experiment was performed at a Reynolds number of 1.5×10^5. The freestream air density is used to nondimensionalize the moment of inertia of the wing for the computations. This density is unavailable and so the value was assumed to be $1.23\ \text{kg} \cdot \text{m}^{-3}$ [sea-level International Standard Atmosphere (ISA) conditions]. The CFD solution at an angle of attack of 40 deg and a roll angle of 10 deg is shown in Fig. 2. The leading-edge vortices and the asymmetric breakdown are visualized in the figure, and it is these features that drive the roll instability referred to here as the wing rock.

[¶]Data available online at crd.lbl.gov/dhbailey/mpidist/index.html [retrieved 28 February 2006].

Table 1 Convergence of reduced-order model third Jacobian contribution with finite difference step size $h = 10^{-n}$. These results are on the coarse grid (described below) using the second-order spatial discretization

n	$\text{Re}\langle \mathbf{q}, C(\mathbf{p}, \mathbf{p}, \bar{\mathbf{p}}) \rangle$	$\text{Im}\langle \mathbf{q}, C(\mathbf{p}, \mathbf{p}, \bar{\mathbf{p}}) \rangle$
4	5.5347700126789234e − 01	6.2858220561002369e + 00
6	3.5505862837191756e + 02	2.3350599906148987e + 03
8	3.1526220567128992e + 04	1.6834102453444750e + 05
10	1.9147851302829609e − 04	1.1694372975048235e − 02
12	1.9147851302829441e − 04	1.1694372975048255e − 02
14	1.9147851302817110e − 04	1.1694372975048051e − 02
16	1.9147858912814422e − 04	1.1694373075537749e − 02

Steady-State CFD Tests

Before simulating the wing rock, the accuracy of steady solutions was verified with a grid refinement study. A fine grid for Euler simulations was created with approximately 1.6×10^6 points. From this grid two levels were extracted by removing every second grid point in each direction. The Reynolds-averaged Navier–Stokes (RANS) solution was performed on a grid with a high resolution in the vortical and boundary layer regions. This grid has 1.8×10^6 points. Steady-state solutions were computed for each grid with the residual being reduced by 6 orders of magnitude. The test case chosen for validation purposes has the wing at 30-deg angle of attack and rolled +10 deg.

The upper surface pressure distributions from all three Euler grid levels are shown in Fig. 3 for the chordwise station at $60\%c_r$ and are compared with the measurements of Arena [13]. It should be noted that the experimental results indicated laminar flow on the upper surface of the wing which has the effect of moving the primary vortices inboard and upward off the surface of the wing. This should be kept in mind when considering the wing rock which is attributed to hysteretic vortex movement [12]. Examination of the surface pressure distributions from each grid indicates that the solutions are not grid converged. However, Euler simulations of delta wing flows are known to be highly sensitive to grid density due to the mechanisms for the generation of vorticity which are based on the truncation error of the discretization [13], and therefore the current results are as expected. Despite the requirement to choose an appropriate level of grid density, it is known that Euler simulations can realistically predict the dynamic response of leading-edge vortices. Comparing the surface pressure distributions at $60\%c_r$, there is reasonably good agreement between the solution from the

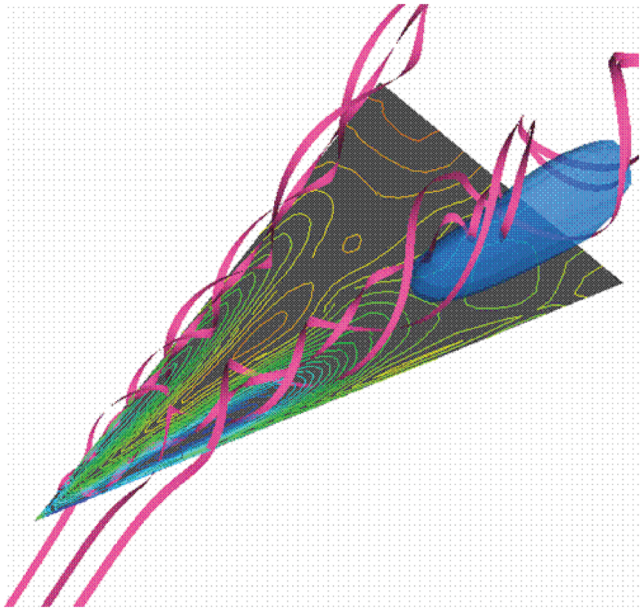

Fig. 2 Picture of the flowfield around the 80-deg wing at an angle of attack 40 deg and a roll angle of 10 deg.

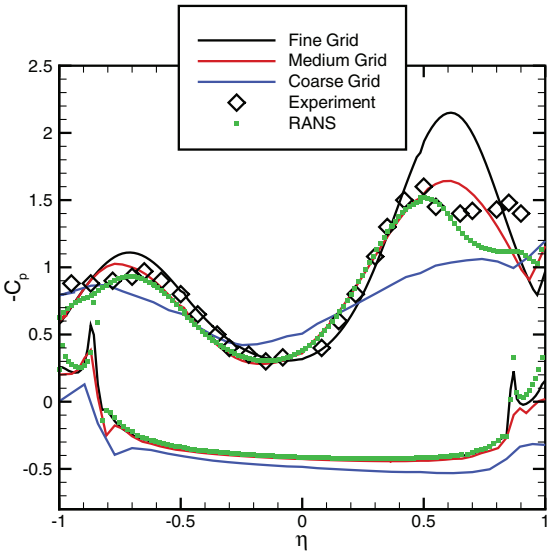

Fig. 3 Grid refinement study–surface pressure distributions at 60%c_r. The lines indicate the coarse, medium, and fine Euler results.

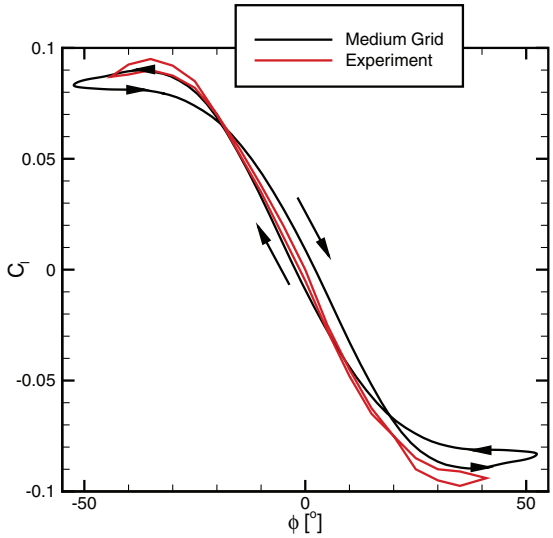

Fig. 4 Comparison of rolling moments through a steady wing-rock cycle: CFD and experiment.

medium grid and experiment. The effect of viscosity can be seen as a drop in the primary vortex suction peaks, which is due to the presence of a secondary separation shifting the primary vortex location away from the wing. As such, the RANS suction peaks and locations compare well with experiment.

Wing-Rock Response

The increase in pressure difference between the port and the starboard sides as the grid is refined induces a stronger restoring moment which is likely to produce a stronger wing-rock response. The wing-rock amplitude at an incidence of 30 deg of incidence on the medium grid is 50 deg with the wing-rock amplitude observed in experiment being 40 deg.

A comparison of the rolling moments from the medium grid and experiment through one complete steady wing-rock cycle is shown in Fig. 4. Despite the maximum roll angle being exceeded in the Euler solution, it is clear that there is reasonably good agreement with experiment, with the rolling moment distribution and magnitudes being predicted well. As discussed by Arena and Nelson [12] there is a clockwise loop where energy is added to the system, and two anticlockwise damping lobes when energy is dissipated. Comparing the width of the loops where energy is added, more energy is being added to the system in the Euler simulations in comparison to experiment. The damping lobes are also larger in the Euler solution in comparison to experiment.

To verify the temporal accuracy of the solutions, a time step refinement study was conducted. It was found that the nondimensional time step of 0.1875 provides an adequate temporal resolution for the current wing-rock studies. This equates to around 120 time steps per cycle. For forced motion studies as few as 50 time steps per cycle are sufficient for temporal convergence; however, because in free-to-roll studies errors amplify with time (autorotation was observed to occur when the time step was too large), a smaller time step is required to accurately predict the wing-rock behavior.

Roll angle histories for Euler and RANS simulations of the 80-deg sweep delta wing at 30 deg angle of attack are shown in Fig. 5. Comparing first the wing-rock amplitudes, the amplitudes from the RANS solution, Euler solution, and experiment are 35, 50, and 40 deg, respectively. Clearly the effect of viscosity is to reduce the wing-rock amplitude. This is as expected based on the previous discussion. With the higher more outboard suction peaks from the Euler solutions there is a much larger wing-rock response in comparison to the RANS solutions, where the suction peaks are lower and more inboard. Comparing the period of the wing-rock cycle we can see that the Euler and RANS solutions produce similar results. As such it is concluded that the Euler solutions predict

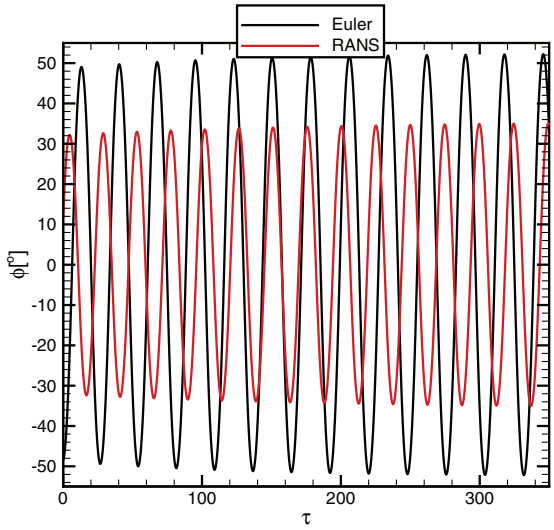

Fig. 5 Effect of modeling: comparison between RANS and Euler solutions for $\alpha = 30$ deg.

qualitatively the correct vortex dynamics and therefore gives a realistic wing-rock response for the purposes of testing the fast prediction methods.

Onset Angle

Simulations of free-to-roll motion of the 80-deg wing at 15- and 20-deg angle of attack were conducted on the medium grid using the Euler equations. At 15-deg angle of attack the solution is dynamically stable (i.e., the amplitude of the oscillations decreases due to aerodynamic damping). However at 20-deg angle of attack, the initial roll angle of 10 deg initiates a wing-rock response with the amplitude of the motion increasing with time. The onset of the wing rock observed in experiment was 22 deg [12].

Results

Results are presented in this section in the following order. First, the coarse grid IPM calculations could be done on a single processor and so sequential performance could be obtained as a benchmark for the parallel method. Sequential and parallel comparisons are shown first for the coarse grid. Then IPM results are obtained in parallel for the medium grid. Finally, reduced model predictions of the limit

cycle oscillation (LCO) growth are shown. These were obtained on the coarse grid as the parallel version of the code to generate the model coefficients has yet to be developed.

Coarse Grid Tests

As a first test of the second-order Jacobians and the linear solver, the IPM was used to calculate the wing-rock onset angle on the coarse grid. Three levels of fill-in were used for the preconditioner which allowed the residual of the linear system to be driven down 11 orders in less than 60 iterations.

At 22 deg, after seven inverse power iterations, the critical eigenvalue had converged to six significant figures. The value is $-1.381245 \times 10^{-4} \pm i0.223497$. At 23 deg, the converged value is $1.805895 \times 10^{-4} \pm i0.232095$. These angles bracket the onset angle, which can be estimated by linear interpolation as 22.4 deg. This is in agreement with the results of other methods for the coarse grid [7].

Next, the use of the first-order Jacobian to calculate the preconditioner for the linear system which uses the second-order Jacobian is examined. The system used to test the linear solver was generated at 21-deg incidence. There are two preconditioners used: the BILU factorization with one, two, and three levels of fill-in, and the polynomial preconditioner combined with BILU(2). The calculations shown in Fig. 6 were done on one processor and so the BILU factorization involves no extra approximation to allow efficient parallel calculation. We first evaluate the results in terms of iterations to convergence because we are ultimately concerned with how the performance of the Krylov method scales in parallel. The number of iterations to convergence reduces as expected as the level of fill-in is increased. The number of iterations in each case is significantly larger than when the preconditioner is calculated for the second-order Jacobian matrix, when three levels of fill-in are required. The increase in the number of iterations is from 60 to 168 although each iteration is around twice as expensive for the second-order matrix preconditioner. Using the polynomial preconditioner on top of BILU(2) in this case does nothing to change the number of iterations to convergence.

The cost of computing the eigenvalues in terms of multiples of the steady-state CFD calculation cost is 2.80 for BILU(0), 2.34 for BILU (1), 2.44 for BILU(2), and 3.70 for the polynomial preconditioner in addition.

Next we test the scaling of the methods in parallel. Here the BILU factorizations are blocked on each processor and it is the influence of this that is the key concern. The convergence using BILU(2) with and without polynomial preconditioning on one and four processors is shown in Fig. 7. The number of iterations using the BILU preconditioner roughly doubles between one and four processors. Using the polynomial preconditioner actually reduces the number of iterations to convergence when moving from one to four processors. These results are encouraging in the sense that the polynomial preconditioner is bringing in enough global information about the solution of the system to allow scaling to larger numbers of processors.

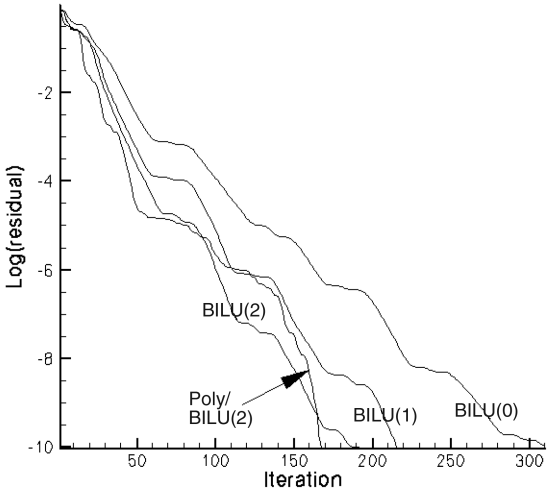

Fig. 6 Linear solver convergence for BILU(k) and polynomial/BILU (2) on the coarse grid and one processor.

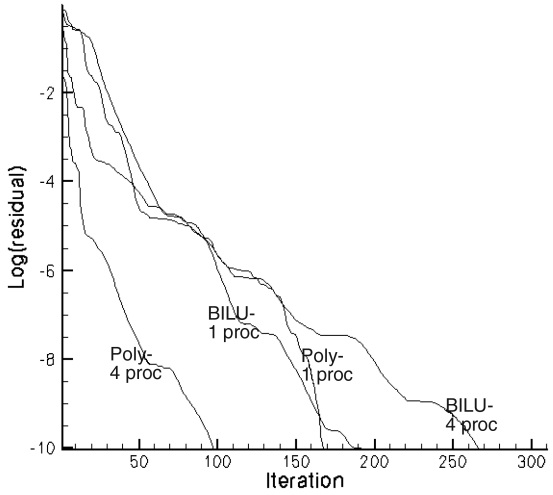

Fig. 7 Linear solver convergence for BILU(2) and polynomial/BILU (1) on the coarse grid and 1 and 4 processors.

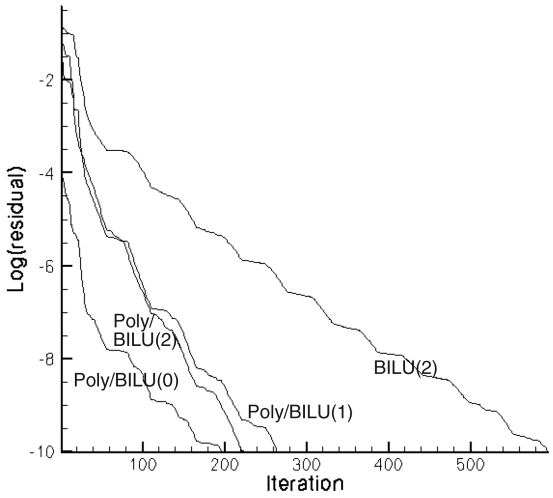

Fig. 8 Linear solver convergence for BILU(2) and polynomial/BILU (k) on the medium grid and 16 processors.

Medium Grid Tests

The test of the parallel solver is whether the medium grid can be solved, which it cannot be in serial because of the memory requirements of the method (estimated 5.6 GB on this grid to store the Jacobian and preconditioner). To evaluate this, the medium grid was calculated on 16 processors. The convergence of the linear solver is shown in Fig. 8. The system used here was generated at 15-deg incidence.

First the BILU(2) results are shown for reference and the performance of the linear solver becomes very poor due to the localization of the preconditioner on each processor. The polynomial preconditioner significantly cuts the number of iterations to convergence. Results are shown using different levels of fill-in, and the number of iterations to convergence cluster between 200 and 260 iterations. The number of iterations will inevitably increase as the size of the grid increases, even sequentially.

The performance of the IPM is summarized in Table 2. First, the improvement in the performance of the linear solver from using the polynomial preconditioner is clear. The number of linear solver steps

Table 2 Summary of timings on medium grid on 16 processors

α	CPU polynomial	CPU BILU(2)	Linear polynomial	Linear BILU(2)	Eigenvalue
15 deg	2.91	3.80	229	596	$\pm 0.172i - 7.53 \times 10^{-4}$
16 deg	2.53	4.08	214	641	$\pm 0.183i - 2.25 \times 10^{-4}$
17 deg	2.31	4.00	202	704	$\pm 0.192i + 2.01 \times 10^{-4}$
18 deg	2.69	4.38	265	774	$\pm 0.202i + 6.32 \times 10^{-4}$

to convergence is reduced by roughly a factor of 3. The resulting improvement in the time to convergence of the IPM is roughly 25–40%. Finally, the table shows that the bifurcation happens between 16 and 17 deg. This is consistent with the prediction of the time domain solver.

Limit Cycle Results

Finally, the reduced model predictions for the second-order spatial scheme on the coarse grid were calculated. Currently the code to carry out the extended accuracy arithmetic matrix free products is not implemented in parallel and so the reduced model could not be generated on the medium grid due to memory limitations. The growth of the limit cycle oscillation compared with time domain results is shown in Fig. 9. For the full-order (150,000 degrees of freedom) predictions the calculations took 1–2 days to settle to a limit cycle oscillation. The reduced model predictions (2 degrees of freedom) were obtained almost instantaneously for any angle after the reduced model coefficients were derived, an operation that takes no more than 30 min using a laptop for this grid. The comparison is excellent within a few degrees of the wing-rock onset angle and gradually becomes worse as the angle of attack becomes larger. It is expected that the Taylor series and center manifold approximations will become worse as we move away from the bifurcation point. However, the most useful information is close to the onset angle, and the reduced model predicts well the expected amplitude immediately after the onset angle is passed.

The parallel implementation of the generation of the reduced order requires extended order accuracy residual evaluations and solutions of linear systems are very similar to that of the IPM. This will be done as future work.

Conclusions

Two aspects of the prediction of flight mechanics instabilities driven by nonlinear aerodynamics were considered in this paper. The wing rock of an 80-deg delta wing was considered as a test case.

First, the wing-rock onset angle was calculated by considering the eigenvalue behavior of the discrete Jacobian matrix. The eigenvalues were computed using the IPM. The parallel implementation of the IPM was considered, and particularly the preconditioning of the Krylov linear solver. The baseline method is BILU factorization with varying levels of fill-in. When implementing this in parallel a reduction in performance arises from making the BILU factorization local. It was proposed to use polynomial preconditioning on top of blocked BILU factorization to bring more global information into the preconditioning. Results showed that this was effective in maintaining the number of Krylov iterations to convergence, even if the operations associated with the preconditioning are more expensive.

Calculations of the onset angle were successfully carried out on the medium grid on 16 processors (in parallel for the first time). The performance of these calculations showed that the eigenvalue at each angle of incidence could be computed in a computational cost between 2 and 3 times the cost of a steady-state CFD calculation.

Secondly, the use of a projection onto the critical eigenvector was shown to produce a 2-degrees-of-freedom model which can predict the rise of the limit cycle amplitude as the onset angle is exceeded.

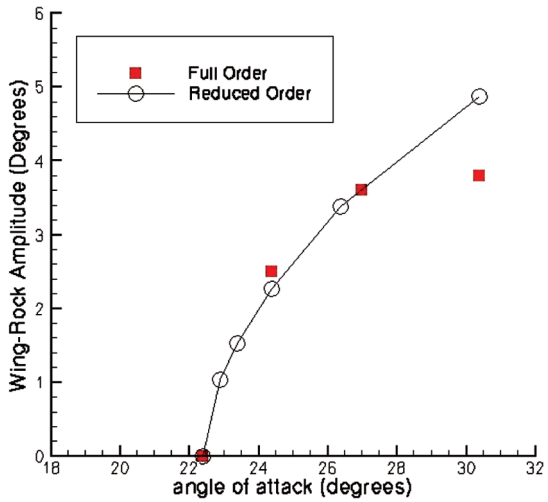

Fig. 9 Comparison of the predicted wing-rock amplitudes of the full-order and reduced-order models on the coarse grid using a first-order spatial discretization.

Acknowledgments

This work was sponsored by the U.S. Air Force Office of Scientific Research, Air Force Material Command, USAF, under grant number FA8655-06-1-3033. The U.S. Government is authorized to reproduce and distribute reprints for government purpose notwithstanding any copyright notation thereon. The views and conclusions contained herein are those of the authors and should not be interpreted as necessarily representing the official policies or endorsements, either expressed or implied, of the U.S. Air Force Office of Scientific Research or the U.S. Government.

References

[1] Lee-Rausch, E. M., and Batina, J. T., "Conical Euler Analysis and Active Roll Suppression for Unsteady Vortical Flows About Rolling Delta Wings," NASA Techical Paper 3259, 1993.

[2] Chaderjian, N. M., and Schiff, L. B., "Numerical Simulation of Forced and Free-To-Roll Delta Wing Motions," *Journal of Aircraft*, Vol. 33, No. 1, Jan.–Feb. 1996, pp. 93–99.

[3] Arthur, M. T., Allan, M., Ceresola, N., Kompenhans, J., Fritz, W., Boelens, O. J., and Pranata, B. B., "Exploration of the Free Rolling Motion of a Delta Wing Configuration in a Vortical Flow," RTO-MP-AVT-123, NATO RTO, Hungary, 2005

[4] Soemarwoto, B., Boelens, O., Fritz, W., Allan, M., Ceresola, N., and Buetefisch, K., "Towards the Simulation of Unsteady Maneuvers Dominated by Vortical Flow," AIAA Paper 2003-3528, 28–26 June 2003.

[5] Saad, A. A., "Simulation and Analysis of Wing Rock Physics for a Generic Fighter Model with Three Degrees-Of-Freedom," Ph.D. Dissertation, Air Force Institute of Technology, Wright–Patterson Air Force Base, Dayton, OH, July 2000.

[6] Morton, S. A., and Beran, P. S., "Hopf-Bifurcation Analysis of Airfoil Flutter at Transonic Speeds," *Journal of Aircraft*, Vol. 36, No. 2, 1999, pp. 421–429.

[7] Badcock, K. J., Woodgate, M. A., and Beran, P. S., "CFD Based Wing Rock Stability Analysis using Time Marching, Reduced Modelling and Hopf Bifurcation Methods," *International Forum on Aeroelasticity and Structural Dynamics*, Deutsche Gesellschaft fur Luft-und Raumfahrt, Munich, July 2005.

[8] Woodgate, M. A., and Badcock, K. J., "On the Fast Prediction of Transonic Aeroelastic Stability and Limit Cycles," *AIAA Journal*, Vol. 45, No. 6, 2007, pp. 1370–1381. doi:10.2514/1.25604

[9] Badcock, K. J., Richards, B. E., and Woodgate, M. A., "Elements of Computational Fluid Dynamics on Block Structured Grids Using Implicit Solvers," *Progress in Aerospace Sciences*, Vol. 36, Nos. 5–6, 2000, pp. 351–392.
doi:10.1016/S0376-0421(00)00005-1

[10] Golub, G. H., and Van Loan, C. F., *Matrix Computations*, The John Hopkins University Press, Baltimore, MD, 1996.

[11] Eisenstat, S. C., Elman, H. C., and Schultz, M., "Variational Iterative Methods for Nonsymmetric Systems of Linear Equations," *SIAM Journal on Numerical Analysis*, Vol. 20, No. 2, April 1983, pp. 345–357.
doi:10.1137/0720023

[12] Arena, A. S., and Nelson, R. C., "Experimental Investigations on Limit Cycle Wing Rock of Slender Wings," *Journal of Aircraft*, Vol. 31, No. 5, Sept.–Oct. 1994, pp. 1148–1155.

[13] Arena, A., "An Experimental and Computational Investigation of Slender Wings Undergoing Wing Rock," Ph.D. Thesis, University of Notre Dame, Notre Dame, IN, April 1992.